Electrical conduction in nanoceramic PGT synthesised by high energy ball milling

SKS Parashar[1*]
[*] Corresponding author
Email: sksparashar@yahoo.com

Swarat Chaudhuri[2]
Email: swarat@sxcran.org

Satyendra Narayan Singh[3]
Email: snsphyru@gmail.com

Mahmood Ghoranneviss[4]
Email: ghoranneviss@gmail.com

[1] School of Applied Sciences, KIIT University, Bhubaneswar, Odisha 751024, India

[2] Department of Physics, St. Xavier's College, Ranchi University, Ranchi 834001, India

[3] Department of Physics, Ranchi University, Ranchi 834008, India

[4] Plasma Physics Research Center, Islamic Azad University, Tehran 1477893855, Iran

Archive of SID

Abstract

Nanocrystalline $Pb_{1-3x/2}Gd_xTiO_3$ (where $x = 0.01$) abbreviated as PGT has been synthesised by high energy ball milling at room temperature. X-ray analysis shows that single-phase tetragonal structure of nanocrystalline PGT was formed after 15-h milling. The average crystallite size was found to be 17 nm. The frequency-dependent AC conductivity of the PGT ceramic was studied in the range 100°C to 525°C. Complex impedance analysis suggested the dielectric relaxation to be of non-Debye type. The activation energy was found to be 1.04 ev. The mechanism of charge transport in nanocrystalline PGT was successfully explained by correlated hopping model.

Keywords

Nanocrystalline, High energy ball milling, Complex impedance spectroscopy, Activation energy, Correlated barrier hopping

Background

Lead titanate ($PbTiO_3$) is a well known ferroelectric ceramic having perovskite structure (ABO_3) with the Pb^{2+} ions at the cell corner A sites, Ti^{4+} ions occupying the body centre B

www.SID.ir

sites and the oxygen atoms at the face centre sites. The perovskite structure has an intrinsic capability to host ions of different sizes, and a wide variety of elements can be accommodated into the structure considering several factors namely (a) charge neutrality, (b) tolerance factor, (c) ionic radius and (d) solubility [1]. It is a well-known ferroelectrics which has several industrial applications like piezoelectric, capacitor, transducer and memory devices [1]. Detailed literature survey reveals that structural and electrical properties of lead titanate (PT) ceramics can be modified by addition of lanthanide ions [2]. A high energy ball milling (HEBM) technique has successfully been used to synthesise nanocrystalline ferroelectrics and other alloys [3,4]. Though nanocrystalline ceramics can be synthesised by a range of different physical, chemical and mechanical methods, HEBM offers several advantages over the other methods [5-7]. The superiority of HEBM over high-temperature solid state reaction technique/wet chemical process is because it lowers the calcinations and sintering temperature due to atomic or molecular scale homogeneity of the synthesised nanocrystalline powders. HEBM is a very useful process to prepare lead-based ceramics [8] and others because it takes place close to a room temperature, thus effectively alleviating the loss of PbO.

The study of electrical conductivity in the ferroelectric compounds is very important since the associated physical properties like dielectric, pyroelectric and piezoelectric are dependent on the nature and magnitude of conductivity of the materials. Moreover, complex impedance spectroscopy technique can be considered as a powerful experimental technique in order to correlate the electrical and structural characteristics in ceramics. This technique has been successfully used to understand the dielectric behaviour of single crystal, polycrystalline and amorphous ceramic materials [9]. It is the most commonly used experimental technique to analyse the dynamics of the ionic movement in ceramic materials. Contribution of various microscopic elements such as grain, grain boundary and interfaces to the total dielectric response in polycrystalline solids can be identified by an equivalent circuit which contains an array of parallel RC elements [10]. A detailed literature survey suggests that not much work in this direction has been reported so far for nanocrystalline $Pb_{1-3x/2}Gd_xTiO_3$ (PGT). In this present work, PGT nanocrystalline ceramics were prepared using HEBM at room temperature. The investigation of dielectric relaxation and electrical conduction properties of nanocrystalline PGT are reported. An attempt has also been made to explain the conduction mechanism in PGT using complex impedance spectroscopy. The correlated barrier hopping model has been applied to the AC conductivity data to understand the conduction mechanism of charge transport in the system. The AC conductivity data were used to estimate the apparent activation energy, density of states at Fermi level and minimum hopping length.

Results and discussion

Structures and microstructures

Figure 1 shows the XRD pattern of PGT subjected to different durations of milling. Most of the XRD peaks of PGT were identified and indexed in tetragonal crystal system using X-pert High Score Plus (PANalytical B.V., The Netherlands). A unit cell of PGT was selected, and its lattice parameters were refined. The tetragonality ratio (c/a) was found to be 1.0467. The average crystallite size and lattice strain determined using Scherrer's formula [7] were 17 nm and 0.012, respectively.

Figure 1 XRD pattern of PGT nanoceramics with x = 0.01 at different milling times.

Archive of SID

www.SID.ir

Dielectric studies

Figure 2 shows the temperature dependence of dielectric constant (ε) for PGT at 1, 10, and 100 KHz, and 1 MHz. The sample exhibits ε maxima in its curves which correspond to a phase transition from ferroelectric to paraelectric state. The dielectric constant has a maximum value at 470°C for each measured frequency, a temperature lower than 490°C for undoped PT as reported by Kong et al. [11]. It was observed from Figure 2 that the phase transition temperature was independent of frequency, suggesting a non-relaxor behaviour of PGT. The lowering of the transition temperature and the increase in dielectric constant values confirm the incorporation of Gd to the perovskite structure, in correspondence with other reports about the effect of small cation substitution of the Pb^{2+} in the A site with Ca^{2+}, Sr^{2+} and La^{3+} ions [11-13]. In low frequency range, the dielectric constant has a high value which can be attributed to various polarisation effects, namely ionic and dipolar. At high frequency, only electronic polarisation contribution dominates; hence, the dielectric values are less.

Figure 2 Temperature dependence of dielectric constant at different frequencies.

Impedance analysis

The real and imaginary parts of dielectric constant were obtained from the impedance data in a conventional way using the following relations [14]:

$$\varepsilon'(\omega) = \frac{Z''}{\omega C_0 |Z|^2} \tag{1}$$

and

$$\varepsilon''(\omega) = \frac{Z'}{\omega C_0 |Z|^2} \tag{2}$$

where $|Z| = [(Z')^2 + (Z'')^2]^{1/2}$

The AC conductivity data were obtained using a relation

$$\sigma^*(\omega) = \sigma'(\omega) + i\sigma''(\omega) = i\omega\varepsilon_0\varepsilon''(\omega) \tag{3}$$

and the real and imaginary parts of $\sigma^*(\omega)$ were obtained as

$$\sigma'(\omega) = \omega\varepsilon_0\varepsilon''(\omega) \tag{4}$$

and

$$\sigma''(\omega) = \omega\varepsilon_0\varepsilon'(\omega). \tag{5}$$

Archive of SID

www.SID.ir

In the conductivity representation for electronic conduction, the real part $\sigma^{/}(\omega)$ should be constant, and the imaginary part $\sigma^{//}(\omega)$ increases linearly with frequency. The AC electrical conductivity in most of the materials due to localised states is given by

$$\sigma^{/}(\omega) = \sigma_0 + A\omega^s, \tag{6}$$

where σ_0 is the frequency-independent part of AC conductivity, $s(0 \le s \le 1)$ is the index, ω = angular frequency of the applied AC field, $A = \pi N^2 e^2 / 6K_B T(2\alpha)$ is a constant, e is the electronic charge, T is the temperature, α is the polarisability of a pair of sites and N is the number of sites per unit volume among which hopping takes place. Such variation is associated with the displacement of carriers which move within the sample by discrete hops of length R between randomly distributed localised sites. The term $A\omega^s$ can often be explained on the basis of two distinct mechanisms for carrier conduction: (a) quantum mechanical tunnelling (QMT) through the barrier separating the localised sites and (b) correlated barrier hopping (CBH) over the same barrier. In these models, the exponent s is found to have two different trends of variations with temperature and frequency. In QMT, s is predicted to be temperature-independent and is expected to show a decreasing trend with ω:

$$s = 1 + \frac{4}{\log(\omega\tau_0)}, \tag{7}$$

where τ_0 is the characteristic relaxation time. The AC conductivity is expected to be [15]

$$\sigma^{/} = \frac{\pi^4}{24} e^2 \omega K_B T [N(E_f)]^2 \alpha^{-1} R_\omega^4, \tag{8}$$

where α^{-1} is the spatial decay parameter for the localised wave function, and R_ω is the tunnelling length at frequency ω

$$R_\omega = \frac{1}{2\alpha} \ln\left(\frac{1}{\omega\tau_0}\right). \tag{9}$$

Further, if AC conductivity occurs from CBH [16],

$$\sigma^{/} = \frac{\pi}{3} e^2 \omega K_B T [N(E_f)]^2 \alpha^{-5} [\ln(\frac{f_0}{\omega})]^4, \tag{10}$$

where $N(E_f)$ is the density of states at Fermi level, f_0 the photon frequency and α is the localised wave function. The exponent (s) and minimum hopping length (R_{min}) can be expressed as [17,18]:

$$s = 1 - \frac{6K_B T}{W_m} \tag{11}$$

and

Archive of SID

www.SID.ir

$$R_{\min} = \frac{2e^2}{\pi\varepsilon\varepsilon_0 W_m}, \quad (12)$$

where W_m is the binding energy, which is defined as the energy required to remove an electron completely from one site to another site, and ε is the dielectric constant of PGT.

The frequency dependence of real permittivity (ε') and imaginary permittivity (ε'') are shown in Figure 3a,b. Both the curves show a decreasing trend with increase in frequency. Dielectric materials have a high dielectric constant at lower frequencies due to space charge contribution. This is evident from the graph of ε' and frequency, where the dispersive nature with relatively high dielectric constant is observed at lower frequency site.

Figure 3 Temperature dependence of (a) real and (b) imaginary dielectric constants at different frequencies.

The dipoles follow the field at low frequencies, and as the frequency increases, the dipoles begin to lag behind the field. At very high frequencies, the dipoles can no longer follow the field, and the value of ε' decreases.

The variation of real Z' and imaginary part of impedance Z'' vs. frequency plot is given in Figure 4(a,b). It can be seen that the curves are temperature-dependent, and the sharpness decreases with increase in temperature. The decrease in magnitude of Z' with increase in frequency for all temperatures indicates an increase in AC conductivity with rise in frequency. The Z' values for all temperatures merge at high frequency due to the release of space charge as a result of reduction in barrier properties of the material with rise in temperature [10] and may be a responsible factor for the enhancement of AC conductivity of the material with temperature at high frequencies. The decrease in Z' values at low frequency with increase in temperature shows a negative temperature coefficient of resistance similar to that of semiconductors. It can also be seen from Figure 4a that the Z' value gives a dip at high frequency and decreases with increase in temperature which may be due to charge carrier hopping (correlated barrier hoping CBH). Figure 4b shows the variation of imaginary part of impedance (Z'') with frequency. The frequency corresponding to the maximum impedance (complex part) shifts towards the right with increase in temperature.

Figure 4 Plots of (a) real and (b) imaginary parts of impedance with different frequencies.

This shift is mainly due to the reduction in bulk resistance with temperature. The broadening of the peaks suggests that there is a spread of relaxation times. The significant broadening of peaks on increasing temperature suggests the presence of a temperature-dependent relaxation process in the materials. The relaxation species may be possibly electrons at low temperature and defects at higher temperature. In the case of dielectric materials, the localised relaxation dominates [19] (i.e. defect relaxation) because of a low dielectric ratio r ($r = \frac{\varepsilon_s}{\varepsilon_\infty}$), where ε_s and ε_∞ are the dielectric constants at low and high frequencies, respectively.

For the sample under study, the value of r at T_c is calculated to be 1.52 at frequencies 1 KHz and 1 MHz. Figure 5 shows the variation of real (Z') and imaginary (Z'') parts of impedance at different temperatures.

Archive of SID

www.SID.ir

Figure 5 Plot of real part of impedance ($Z^{/}$) with imaginary part of impedance ($Z^{//}$) of PGT.

It is well known that complex impedance analysis helps in understanding the nature of dielectric relaxation in the material [20] as well as grain and grain boundaries in ceramics. For Debye-type relaxation, the centre of the semicircular plots should be located on the Z' axis, whereas for a non-Debye-type relaxation, the Argand plane plots are close to the semicircular arcs with the centre below the real axis. The impedance spectrum for PGT sample consists of two semicircular arcs (Figure 5), which exhibit some degree of decentralisation. This decentralisation or non-Debye relaxation obeys the Cole-Cole formalism [21], where the depressed semicircle represents typically a phenomenon with a spread of relaxation time. The Cole-Cole formalism is given by

$$Z^{*}(\omega) = \frac{R}{1 + \left(j\omega / \omega_0 \right)^{1-n}},$$

where n represents the magnitude of deviation of the electrical response from the ideal condition, and this can be determined from the location of the centre of the semicircles; ω_0 is the frequency at the maximum of the semicircle.

The exponent $n \rightarrow 0$ (i.e. $1 - n = 1$) in the above equation gives the classical Debye formalism. This non-ideal behaviour may happen due to the presence of distributed elements in the material electrode system [13]. The semicircular pattern in the impedance spectrum is representative of the electrical processes taking place in the material which can be thought of as resulting from the cascading effect of a parallel combination of resistive and capacitive elements arising due to the contribution of the bulk property of the material and the grain boundary effects. The high-frequency semicircle is due to the bulk property of the material (parallel combination of bulk resistance and bulk capacitance), and the low-frequency semicircle is due to the grain boundary effects (parallel combination of grain boundary resistance and capacitance). The absence of a third semicircle shows that the electrode material interface contribution to impedance is negligible.

It is clear from Figure 5 that with increase in temperature, the radius of the semicircular arc shifts towards the left side; thus, the bulk resistance R_b decreases with an increase in temperature. It is observed that at temperatures 375°C and above, two semicircles can be traced with different values of grain (R_b) and grain boundary (R_{gb}), and their values can be obtained from the intercept of the traced semicircles with $Z^{/}$ axis. The decrease in the values of R_b with temperature indicates negative temperature coefficient of resistance and is in confirmation with Figure 4a.

AC and DC conductivity

Figure 6a,b shows the log-log plot of real and imaginary parts of AC electrical conductivity. The plots of $\sigma^{/}$ show dispersion throughout the chosen frequency range, and with the increment in temperature, the lines get flattened. Translation from long range hopping to short range ion motion is evident from the switchover from frequency-independent to the frequency-dependant region which also shows the beginning of the conductivity relaxation. The values of s were obtained from the slopes of $\sigma^{/}$-f plots in the low-frequency region.

Archive of SID

www.SID.ir

Figure 6 Log-log plot of (a) real and (b) imaginary parts of AC electrical conductivity with frequencies.

Figure 7 shows the temperature dependence of *s*, and it is also evident from the slopes that the values of *s* are always less than 1 and decrease with the rise in temperature. The value of *s* approaches 0 at higher temperatures, indicating the domination of DC conductivity at higher temperatures in the low-frequency region following Equation (1).

Figure 7 Variation of index *s* with temperature.

The model based on correlated hopping of electrons over barrier predicts a decrease in the value of the index *s* with the increase in temperature, so it is consistent with the experimental results. Thus, the conduction in the system may be due to the short-range translational type hopping of charge carriers. This indicates that the conduction process is a thermally activated process. Materials with high density of states a band gap like that of the semiconductors are generally consistent with hopping conduction mechanism. Due to localisation of charge carriers, the formation of polarons takes place and the hopping conduction may occur between the nearest neighbouring sites.

Figure 8 shows the variation of real part of AC conductivity ($\ln\sigma'$) versus $10^3/T(K^{-1})$ at 1 KHz and 1 MHz. The activation energy for conduction using Arrhenius relationship $\sigma = \sigma_0 \exp(-E_a/kT)$ was obtained as 1.09 and 0.81 eV, respectively, for 1 KHz and 1 MHz. The low value of activation energy suggests a possibility of carrier transport through hopping between localised states in a disordered manner [21].

Figure 8 Variation of $\ln\sigma'$ with inverse of temperature (K^{-1}).

The values of $N(E_f)$ were calculated using Equation (10) by assuming $f_0 = 10^{13}$ Hz and $\alpha = 10^{10}$ m^{-1} at various operating frequencies and temperatures. It can be seen from Figure 9 that the values of $N(E_f)$ decrease with increase in operating frequency and almost merge above 100 KHz. Figure 10 shows the variation of density of states at Fermi level of PGT ceramic with temperature. It is evident from the figure that the density of states increases with temperature for all frequencies. Comparing the two figures (Figures 9 and 10), one can conclude that at low frequencies, the conduction is affected by both frequency and temperature, and at high frequencies, it is affected by thermal excitations since the charges are localised. The high values of $N(E_f)$ are suggestive of hopping between the pair of sites which dominates the conduction mechanism in PGT.

Figure 9 Variation of density of states at Fermi level of PGT ceramic with frequency.

Figure 10 Variation of density of states at Fermi level of PGT ceramic with temperature.

Conclusion

Nanocrystalline Gd-doped lead titanate powders were successfully synthesised by high energy ball milling techniques at room temperature. The frequency-dependent AC conductivity at different temperatures indicated that the conduction process is a thermally activated process. The activation energy calculated from the impedance analysis and the

Archive of SID

www.SID.ir

conductivity data are comparable. At higher temperature, PGT behaves as a semiconductor. The semi-conductivity is attributed to the extra positive charge in the conduction band caused by the substitution of Pb^{+2} ions by trivalent Gd^{+3} ions. With rise in temperature, the donor cations are the major contributors to the conduction process. The donors create an energy level closer to the conduction band, thus reducing the amount of energy required to activate the donors to the conduction band. The correlated barrier hopping model is found to successfully explain the mechanism of charge transport in PGT. The results are well supported by density of states at Fermi level.

Methods

Rare earth gadolinium-modified lead titanate (PGT) nanoceramic with a general formula $Pb_{1-3x/2}Gd_xTiO_3$ (where x was fixed at 0.01) was synthesised from high purity ingredients, PbO, Gd_2O_3 and TiO_2. The starting oxides were mixed in stoichiometric ratio to compensate for the expected Pb loss at high sintering temperatures; 2% extra PbO was used throughout the experiment.

The synthesis of PGT was carried out using high energy ball milling technique. The milling was performed in a planetary ball mill (Retsch PM 200, Retsch, Germany), at room temperature for different milling times (0 to 45 h). The milling was carried out with tungsten carbide (WC) vial and WC balls (with 10-mm diameter) at a speed of 300 rpm and ball-to-powder weight ratio of 15:1. Milling was stopped for 30 min after every 1 h. The phase identification was carried out using an X-ray diffractometer (XRD) (Rigaku with CuKα radiation λ = 0.15418 nm). The powder obtained after 45 h of milling was mixed thoroughly with a 3% PVA and then uni-axially compacted in to disc samples. The discs were formed using a hydraulic pellet press at a pressure of 4 MPa to form pellets of the size of 2 mm in thickness and 10 mm in diameter. The green pellets were sintered at 900°C for 2 h in air atmosphere. The flat polished surfaces of the sintered pellets were electroded with high purity silver paste and then dried at 700°C for 15 min before making any electrical measurements. The electrical parameters were measured using a HIOKI-3532 LCR Hitester (HIOKI, Japan) under a weak electric field (with a maximum magnitude of 1 V) in the temperature range of 100°C to 525°C at different frequencies varying from 10^2 to 10^6 Hz at a heating/cooling rate of 2°C/min.

Competing interests

The authors declare that they have no competing interests.

Authors' contributions

SKSP carried out the calculations and drafted the manuscript. SC has done the experiments, and SNS provided guidance at various stages of the study. MG also helped in drafting the manuscript. All authors read and approved the final manuscript.

References

1. Lines, ME, Glass, AM: Principles and Applications of Ferroelectrics and Related Materials. Clarendon, Oxford (1977)

Archive of SID

www.SID.ir

2. Brankovic, Z, Brankovic, G, Jovalekic, C, Manjette, Y, Cilense, M, Varela, JA: Mechanochemical synthesis of PZT powders. Mater. Sci. Eng. A **345**, 243 (2003)

3. Parasar, SKS, Choudhary, RNP, Murty, BS: Ferroelectric phase transition in $Pb_{0.92}Gd_{0.08}(Zr_{0.53}Ti_{0.47})_{0.98}O_3$ nanoceramic synthesized by high-energy ball milling. J. Appl. Phys. **94**, 6091 (2003)

4. Fatemi, DJ, Harris, VG, Browning, VH, Kiekland, JP: Processing and cation redistribution of MnZn ferrites via high-energy ball milling. J. Appl. Phys. **83**, 6867 (1998)

5. Koch, CC: Nanostructured Materials: Processing, Properties and Potential Applications. Material Science and Process Technology Series. Noyes Publications, NY (1993)

6. Murty, BS, Ranganathan, S: Novel material synthesis by mechanical alloying/milling. Int. Mater. Rev. **43**, 101 (1998)

7. Suryanarayana, C: Mechanical alloying and milling. Prog. Mater. Sci. **46**, 1 (1998)

8. Kong, LB, Ma, J, Zhu, W, Tan, OK: Phase formation of lead zirconate titanate via high energy ball milling process. J. Alloys Compd. **236**, 242 (2002)

9. Prabhakar, K, Mallikarjun Rao, SP: Complex impedance spectroscopy study on fatigued soft and hard PZT ceramics. J. Alloys Compd. **437**, 302 (2007)

10. Rout, SK, Hussain, A, Lee, JS, Kim, IW, Woo, SI: Impedance spectroscopy and morphology of $SrBi_4Ti_4O_{15}$ ceramics prepared by soft chemical method. J. Alloys Compd. **477**, 706 (2009)

11. Kong, LB, Zhang, TS, Ma, J, Boey, F: Progress in synthesis of ferroelectric ceramic materials via high energy mechanochemical techniques. Prog. Mater. Sci. **53**, 207 (2008)

12. Xu, Y: Ferroelectric Materials and their Applications. North Holland, Amsterdam (1991)

13. Portelles, J, Almodovar, NS, Fuentes, J, Raymond, O, Heiras, J, Siqueiros, JM: A.C. conductivity in Gd doped $Pb(Zr_{0.53}Ti_{0.47})O_3$ ceramics. J. Appl. Phys. **104**, 73511 (2008)

14. Macdonald, JR (ed.): Impedance Spectroscopy Emphasizing Solid Materials and Systems. Wiley, NY (1987)

15. Elliott, SR: A.C. conduction in amorphous chalcogenide and pnictide semiconductors. Adv. Phys. **36**, 135 (1987)

16. Sharma, GD, Roy, M, Roy, MS: Charge conduction mechanism and photovoltaic properties of 1,2-diazoamino diphenyl ethane (DDE) based Schottky device. Mater. Sci. Eng. B **104**, 15 (2003)

17. Mollah, S, Som, KK, Bose, K, Chaudhri, BK: AC conductivity in $Bi_4Sr_3Ca_3Cu_yO_x$ (y=0–5) and $Bi_4Sr_3Ca_{3-z}Li_zCu_4O_x$ (z=0.1–1.0) semiconducting oxide glasses. J. Appl. Phys. **74**, 931 (1993)

Archive of SID

www.SID.ir

18. Salam, R: Trapping parameters of electron defects states in indium tin oxide from a.c. conductivity. Phys. Stat. Sol. A **117**, 535 (1990)

19. Nobre, MAL, Lanfredi, S: Dielectric spectroscopy on $Bi_3Zn_2Sb_3O_{14}$ ceramic: An approach based on the complex impedance. J. Phys. Chem. Solids **64**, 2457 (2003)

20. Gerhardt, R: Impedance and dielectric spectroscopy revisited: distinguishing localized relaxation from long-range conductivity. J. Phys. Chem. Solids **55**, 1491 (1994)

21. Parasar, SKS, Choudhary, RNP, Murty, BS: Electrical properties of Gd-doped PZT nanoceramic synthesized by high energy ball milling. Mater. Sci. Eng. **B110**, 58 (2004)

Archive of SID

www.SID.ir

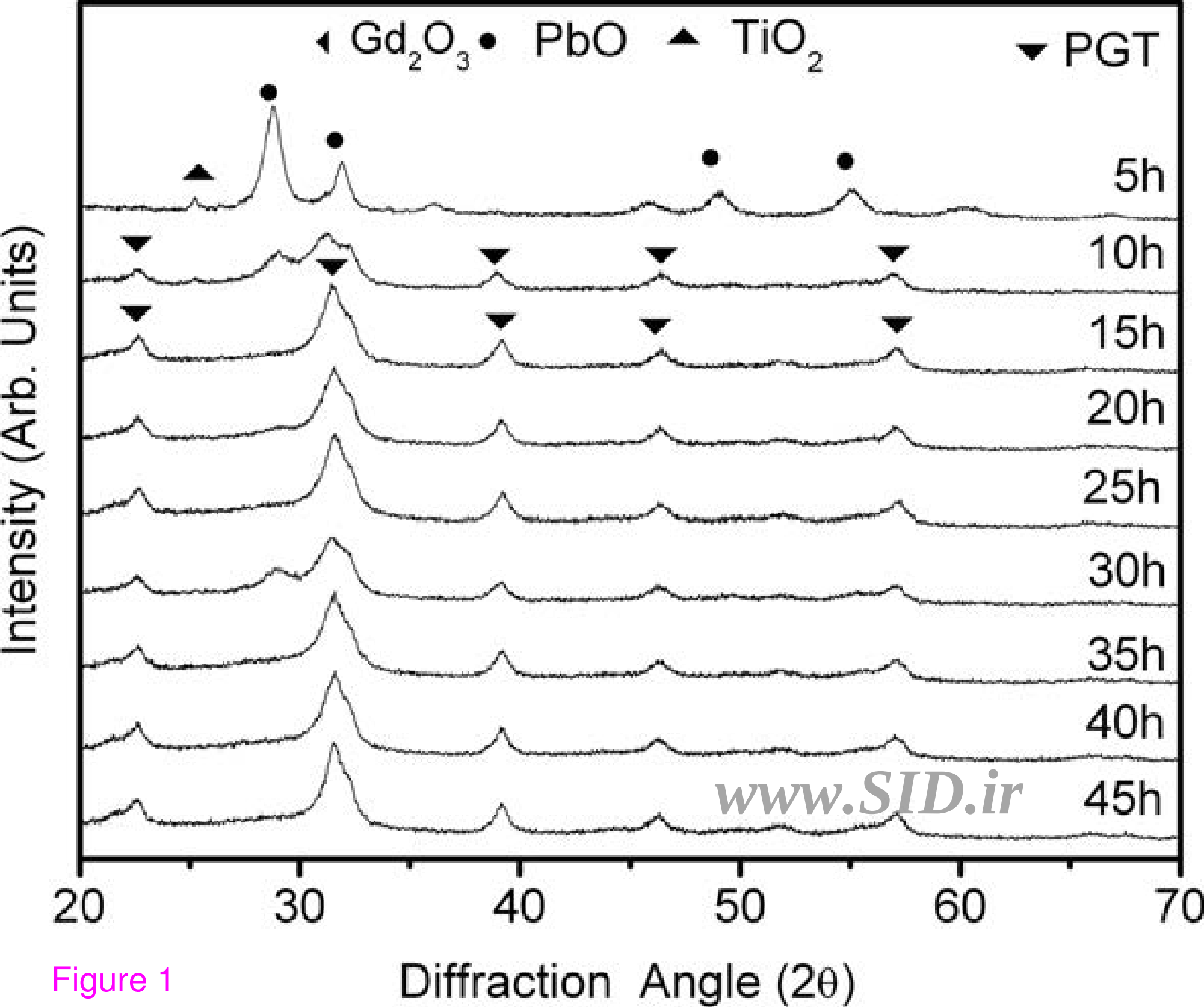

www.SID.ir

Figure 1

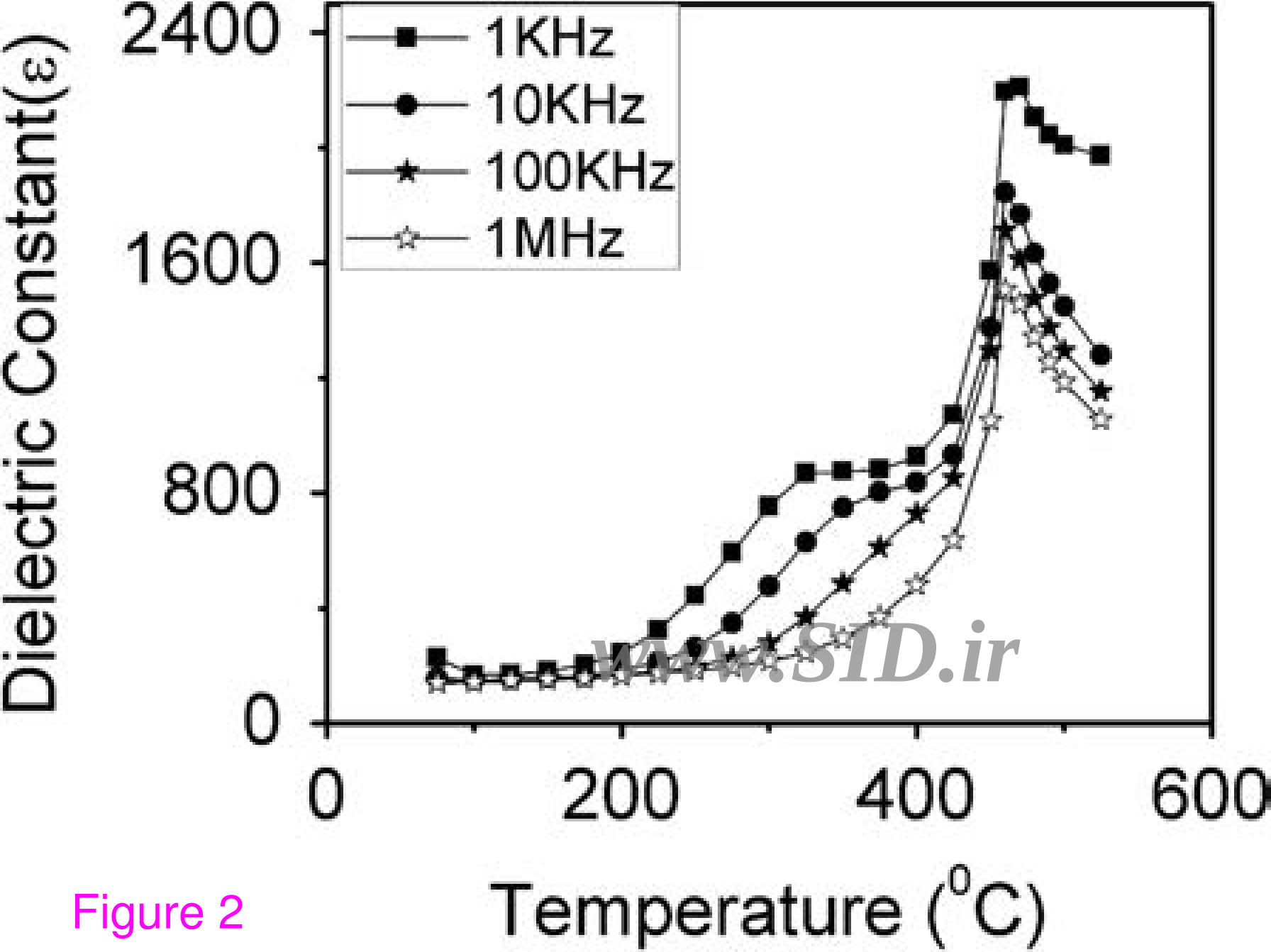

www.SID.ir

Figure 2

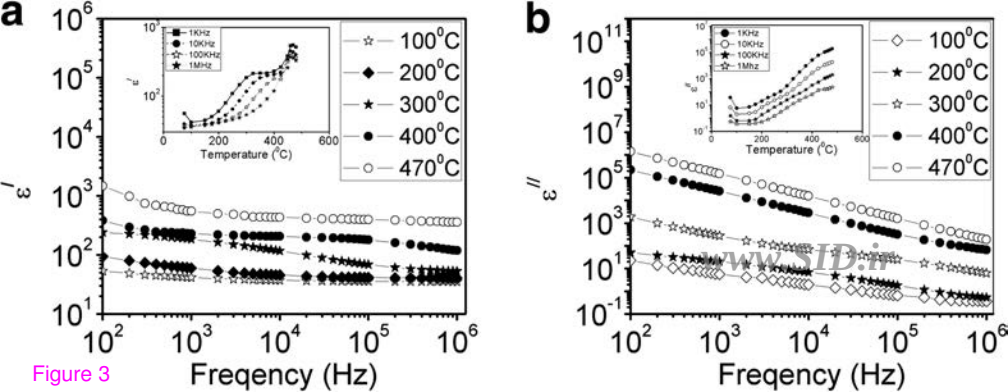
a
b
ε′
ε″
Freqency (Hz)
Temperature (°C)
1KHz
10KHz
100KHz
1Mhz
100°C
200°C
300°C
400°C
470°C
www.SID.ir

Figure 3

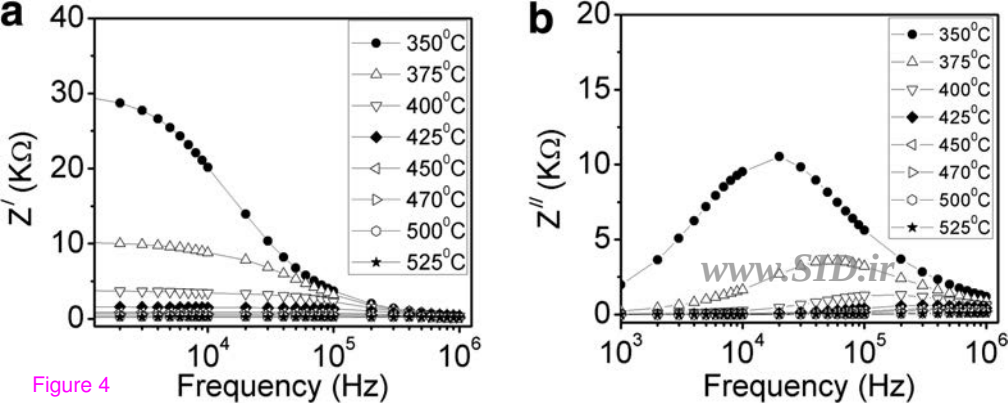
a
b
Z′ (KΩ)
Z″ (KΩ)
Frequency (Hz)
Frequency (Hz)
350°C
375°C
400°C
425°C
450°C
470°C
500°C
525°C
www.SID.ir

Figure 4

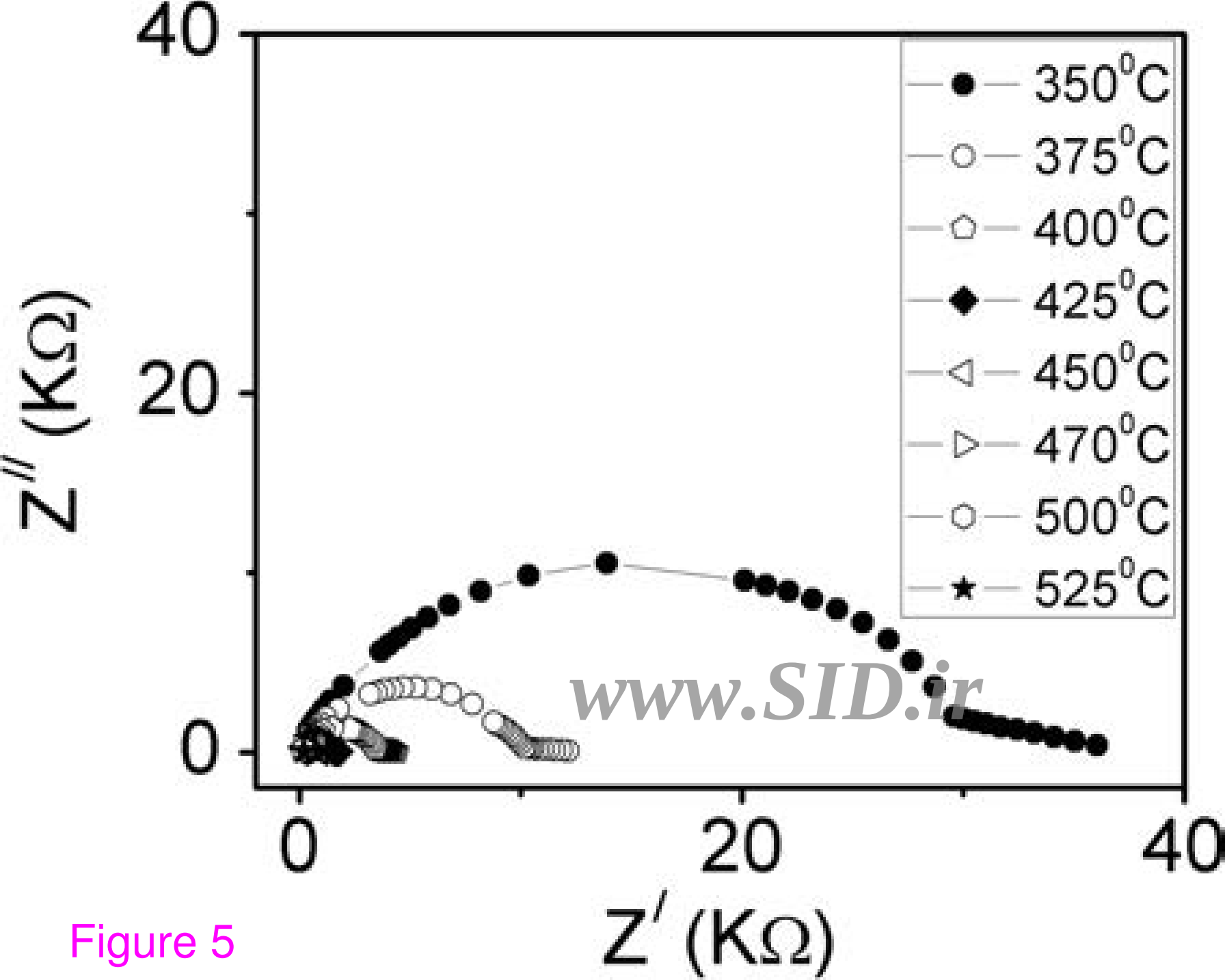

www.SID.ir

Figure 5

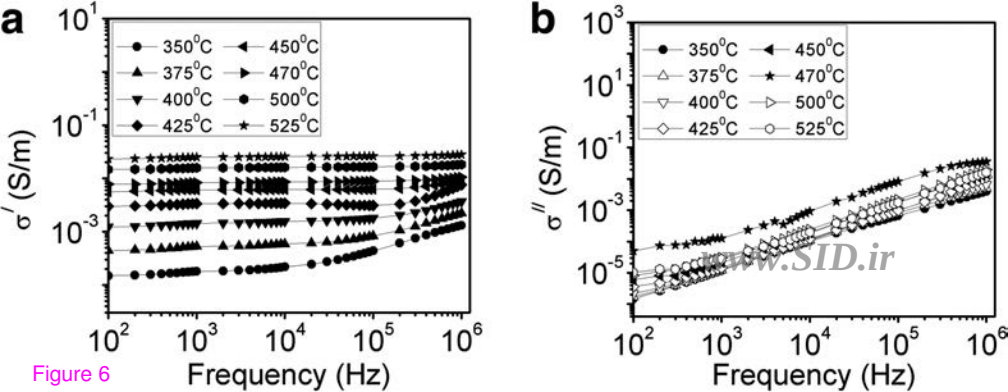
a
b
350°C
375°C
400°C
425°C
450°C
470°C
500°C
525°C
σ′ (S/m)
σ″ (S/m)
Frequency (Hz)
www.SID.ir

Figure 6

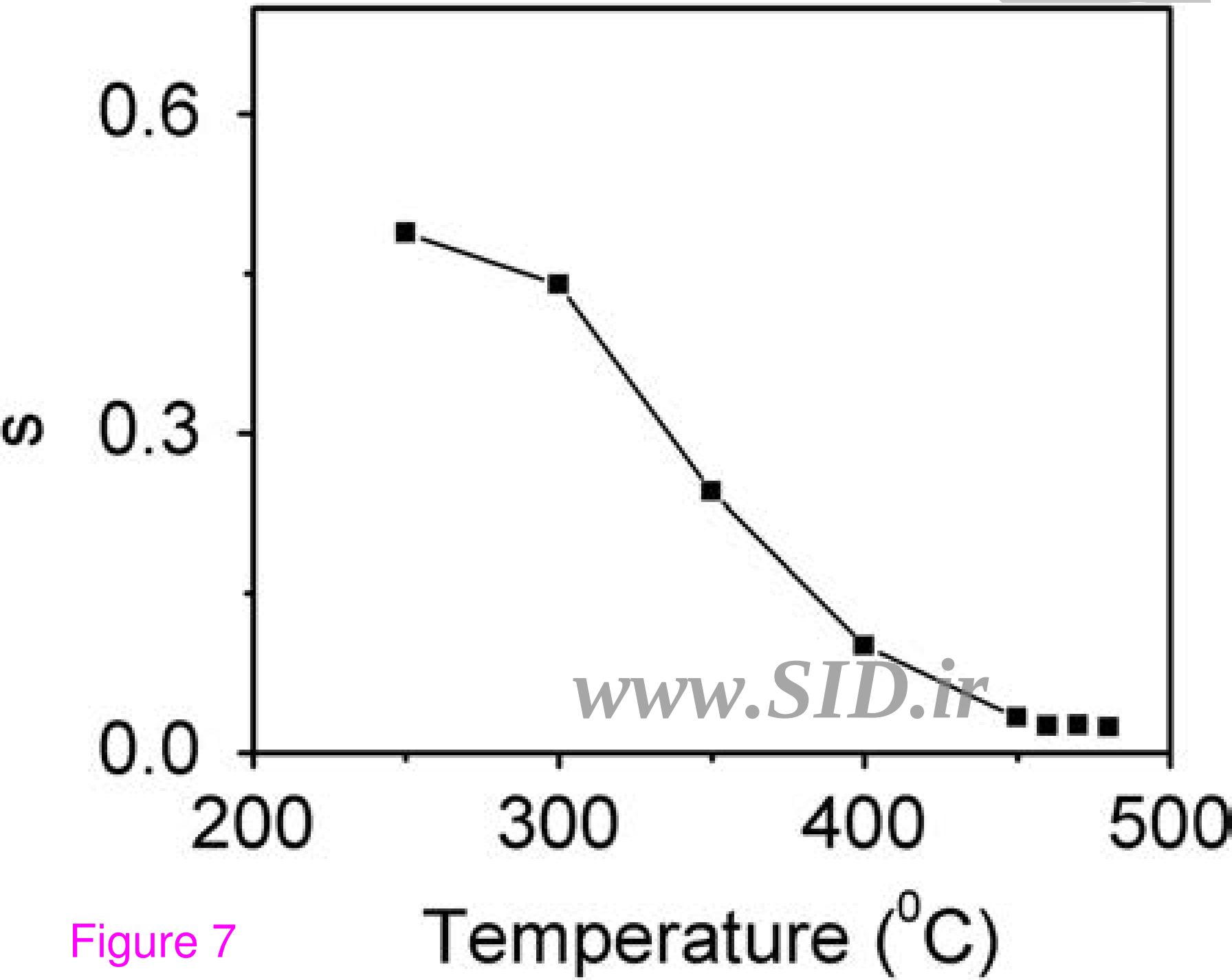

www.SID.ir

Figure 7

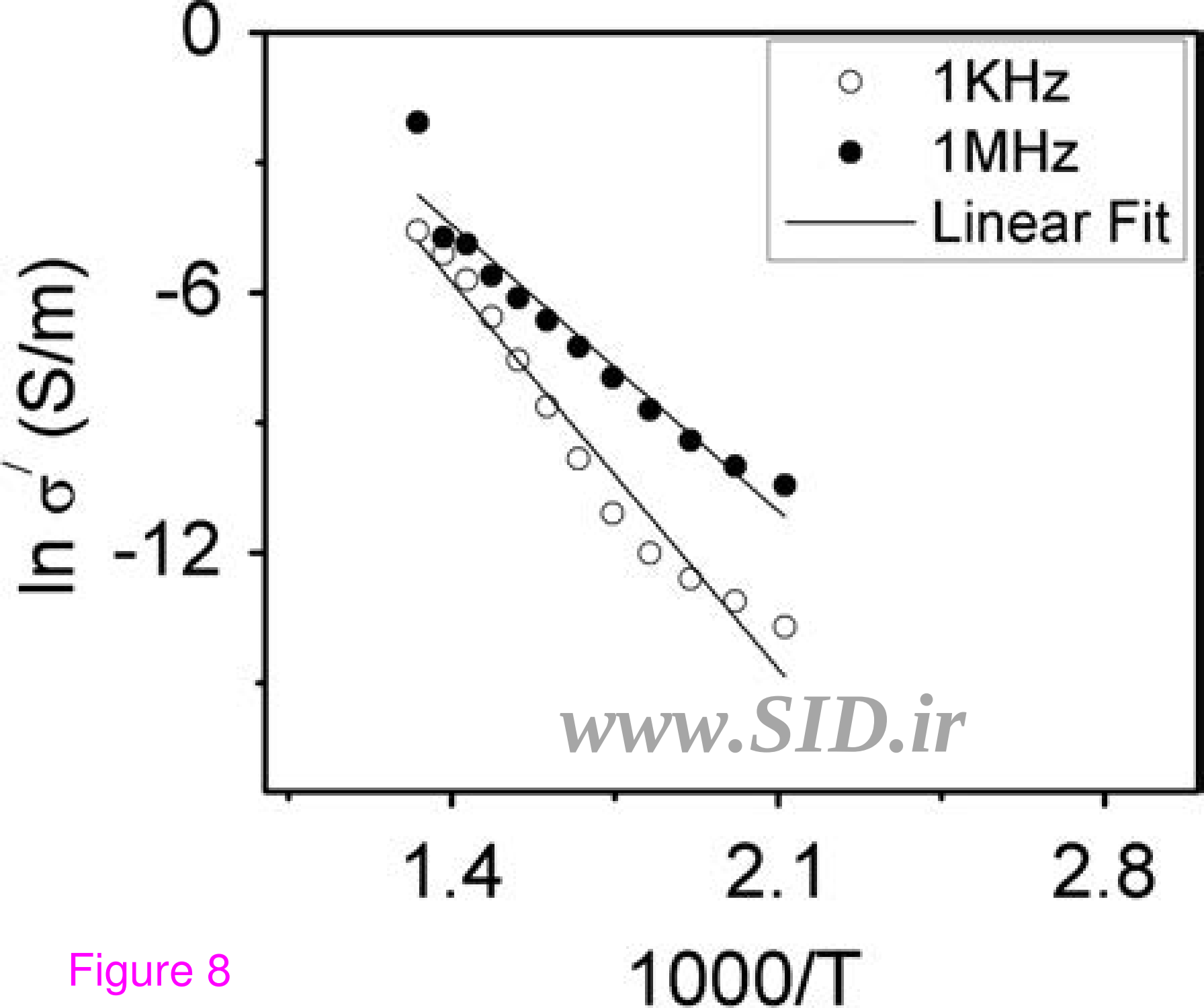

www.SID.ir

Figure 8

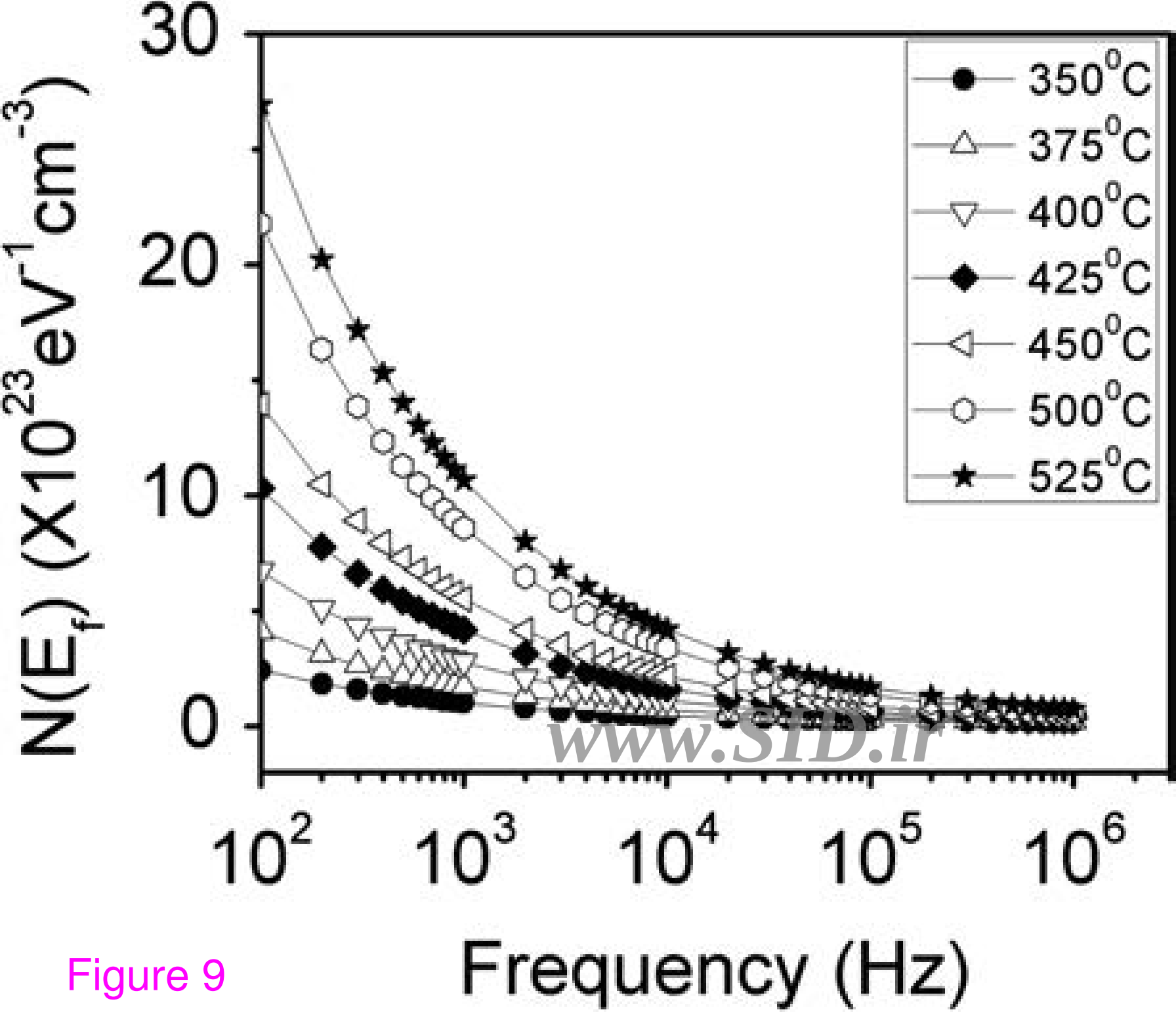

www.SID.ir

Figure 9

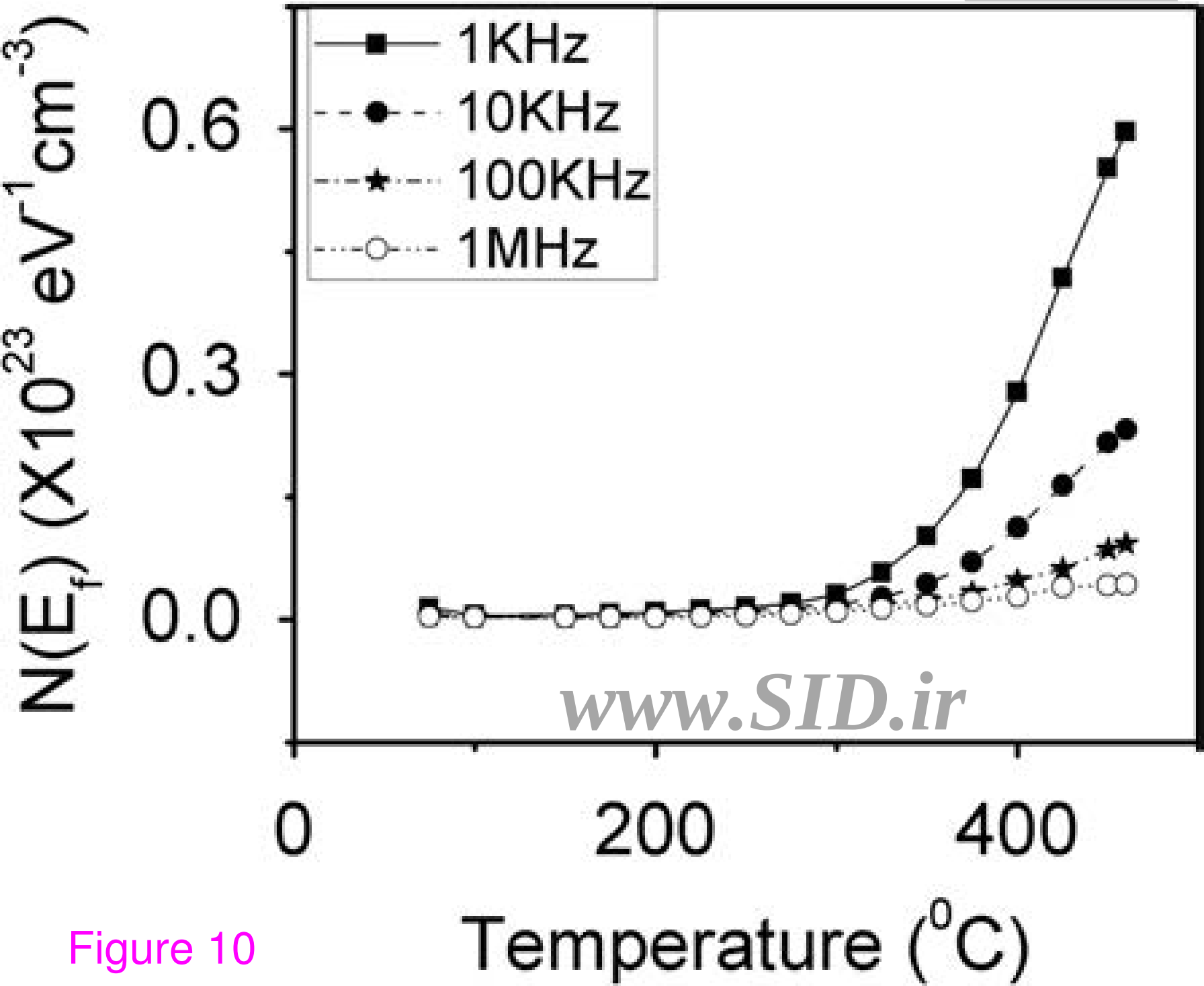
1KHz
10KHz
100KHz
1MHz
0.6
0.3
0.0
N(E_f) (X10^23 eV^-1 cm^-3)
0
200
400
Temperature (°C)
www.SID.ir

Figure 10